Knockdown of hspg2 is associated with abnormal mandibular joint formation and neural crest cell dysfunction in zebrafish

Barbara S. Castellanos
University of Texas at El Paso
Nayeli G Reyes-Nava
University of Texas at El Paso
Anita Quintana (aquintana8@utep.edu)
University of Texas at El Paso https://orcid.org/0000-0002-3596-1587

Research article

Keywords: HSPG2, neural crest cells, craniofacial development

Posted Date: December 30th, 2020

DOI: https://doi.org/10.21203/rs.3.rs-27670/v3

Version of Record: A version of this preprint was published on March 8th, 2021. See the published version at https://doi.org/10.1186/s12861-021-00238-4.

Abstract

Background: Heparan sulfate proteoglycan 2 (*HSPG2)* encodes for perlecan, a large proteoglycan that plays an important role in cartilage formation, cell adhesion, and basement membrane stability. Mutations in *HSPG2* have been associated with Schwartz-Jampel Syndrome (SJS) and Dyssegmental Dysplasia Silverman-Handmaker Type (DDSH), two disorders characterized by skeletal abnormalities. These data indicate a function for *HSPG2* in cartilage development/maintenance. However, the mechanisms in which *HSPG2* regulates cartilage development are not completely understood. Here, we explored the relationship between this gene and craniofacial development through morpholino-mediated knockdown of *hspg2* using zebrafish.

Results: Knockdown of *hspg2* resulted in abnormal development of the mandibular jaw joint at 5 days post fertilization (DPF). We surmised that defects in mandible development were a consequence of neural crest cell (NCC) dysfunction, as these multipotent progenitors produce the cartilage of the head. Early NCC development was normal in morphant animals as measured by distal-less homeobox 2a (*dlx2a)* and SRY-box transcription factor 10 (*sox10)* expression at 1 DPF. However, subsequent analysis at later stages of development (4 DPF) revealed a decrease in the number of $Sox10^{+}$ and Collagen, type II, alpha 1a $(Col2a1a)^{+}$ cells within the mandibular jaw joint region of morphants relative to random control injected embryos. Concurrently, morphants showed a decreased expression of *nkx3.2,* a marker of jaw joint formation, at 4 DPF.

Conclusions: Collectively, these data suggest a complex role for *hspg2* in jaw joint formation and late stage NCC differentiation.

Background

Mutation of the *HSPG2* gene causes Schwartz-Jampel Syndrome (SJS) and Dyssegmental Dysplasia Silverman-Handmaker Type (DDSH) (1–3). SJS is a recessive disorder characterized by muscle stiffness (myotonia) and chondrodysplasia. DDSH is a less frequent but a more severe recessive disorder characterized by reduced joint mobility, severe limb shortening, and short stature (4). Both disorders have common clinical manifestations that include reduced stature, bowing of the long bones, and facial dimorphism (4,5). Interestingly, SJS is generally associated with loss of function mutations in *HSPG2* that vary from missense mutations to splice site mutations. These mutations are dispersed throughout the *HSPG2* protein, with those located closer to the C -terminus being more readily tolerated (5). Conversely, DDSH is caused by homozygous null mutations (frameshifts and point mutations) wherein there is an absence of functional protein, likely due to degradation (5). Despite mutation heterogeneity underlying SJS and DDSH, craniofacial abnormalities such as micrognathia are very common phenotypes in diagnosed patients (5). These manifestations of chondrodysplasia suggest that *HSPG2* plays a role in regulating craniofacial development.

The function of *HSPG2* during chondrogenesis is not completely understood, but is likely related to the various domains within the *HSPG2* protein and the vast array of interactions between *HSPG2* and the extracellular matrix (ECM) to promote signal transduction and stability (6,7). *HSPG2* encodes for perlecan, a large proteoglycan that consists of five domains, each of which have a unique function (8). Four of these domains (domains II, III, IV, and V) have repeats homologous to low-density lipoprotein receptor (domain II), laminins (domains III and V), and immunoglobulins (domain IV), but domain I is unique to perlecan (8). The N-terminal domain I possesses three ser-asp-gly motifs that serve as attachment sites for glycosaminoglycan (GAG) side chains like heparan sulfate (HS) and chondroitin sulfate (CS) (8–10). These side chains facilitate interaction with growth factors such as fibroblast growth factor-2 (FGF-2), vascular endothelial growth factors (VEGFs), and bone morphogenetic proteins (BMPs) (6,10,11) upon secretion of perlecan into the ECM. In addition, HS has been shown to specifically interact with ECM proteins such as fibronectin, laminin, and collagens I, II, III, IV, and V, suggesting perlecan and its side chains mediate cell adhesion and basement membrane stability (12).

As it relates to the chondrocyte phenotypes in SJS and DDSH, previous studies, both *in vitro* and *in vivo*, have established that disrupting *HSPG2* expression leads to abnormal chondrocyte proliferation and disorganized columnar arrangement (13,14). This is significant as chondrocytes are the primary cells found in cartilage and are known to secrete a specialized ECM containing glycoproteins and proteoglycans, like perlecan, in order to maintain structural integrity (15). During craniofacial development, chondrocytes arise from neural crest cells (NCCs), a multipotent progenitor cell population that forms at the dorsal end of the neural tube upon neural tube closure. There are four populations of NCCs, but only cranial NCCs (CNCCs) migrate to the pharyngeal arches and develop into cartilage and bone, making them vital to proper craniofacial development (16–18). These CNCCs are regulated by growth factors like BMP, which are vital for mandibular morphogenesis, and FGFs, which are essential for CNCC differentiation (19–21).

The development of craniofacial bone is due to both endochondral and intramembranous ossification. In endochondral ossification, cells differentiate into chondrocytes and bones develop from a cartilaginous base. This form of ossification necessitates that chondrocytes are present in growth plates where they are arranged into zones of rest, proliferation, and hypertrophy (15,22). These chondrogenic cells play a part in the development of the mandibular jaw joint (also known as the temporomandibular joint or TMJ in mammals) and are derived in part by CNCCs (23). While the TMJ is a synovial joint comprised of the mandibular condyle and glenoid fossa, it develops slightly different than other synovial joints (23). To form the TMJ, CNCCs migrate to the mandibular arch and develop into Meckel's cartilage, which extends out of the mandibular process into the tympanic process. Therefore, middle ear development is tightly intertwined with TMJ development. As with other bone and joint development the Meckel's cartilage is eventually replaced by intramembraneous bone formation. During this process, a blastema, which forms the condylar secondary cartilage (CSC) develops. The CSC is located beneath a thin layer of periosteum (23). The condyle is formed from the secondary cartilage and the periosteal space is made of fibrocartilage, which has a denser ECM than fibrous connective tissue. Ultimately, the fibrocartilage will become an articular disc that divides the fluid filled joint cavity into upper and lower compartments lined

by a soft tissue known as synovium (23). Thus, unlike other synovial joints, the TMJ is formed from CNCCs and the periosteum. In addition, it contains fibrocartilage, which is located in many fewer regions/joints in the body and is distinct because it has a denser ECM than other fibrous tissue. Given the role of ECM and the periosteum in TMJ development, we hypothesized that deletion of perlecan, a primary component of the ECM, would disrupt jaw joint formation.

To begin to test this hypothesis, we performed morpholino mediated knockdown of *hspg2* using the zebrafish model. Apart from general advantages like a high fecundity rate, extra-uterine development, and quick maturation, the zebrafish is an ideal organism to study craniofacial development due to the relative simplicity of the cartilaginous structures of the head and face, all of which are readily visible with stains like Alcian blue (24,25). Most importantly, CNCC development is highly conserved in zebrafish and consequently, suggests that zebrafish are an appropriate model to characterize the function of *hspg2* in craniofacial development (25). Knockdown of *hspg2* resulted in abnormal mandibular jaw joint formation and disrupted late stage differentiation of CNCCs, with little to no effect on early stage CNCC development. Collectively, our results suggest that *hspg2* is essential for joint formation in the developing zebrafish.

Results

Morpholino-induced knockdown of hspg2 is associated with craniofacial phenotypes

It has previously been reported that *hspg2* mRNA is expressed ubiquitously throughout the head, eyes, and somites of the zebrafish. Additional immunohistochemistry staining revealed positive expression of perlecan in these regions from embryos at 2-3 hours post fertilization to 5 days post fertilization (DPF) (26,27). Based on this expression pattern and previous murine studies establishing that mutation of *Hspg2* results in failure of the chondro-osseous junction of developing bones and craniofacial abnormalities (13), we hypothesized that morpholino mediated knockdown of the zebrafish *hspg2* gene would cause craniofacial abnormalities.

We performed Alcian blue staining to detect craniofacial abnormalities in the developing cartilage. We measured the distance from the top of the ceratohyal to the tip of the Meckel's cartilage as a read out for mandibular truncation as previously described (28). Measurements of the distance between the top of the ceratohyal and Meckel's cartilage at 5 DPF (Figure 1A, 1B, and 1C) showed that the injection of the *hspg2* translation blocking morpholino caused a 7% truncation in the zebrafish mandible when compared to the random control group. The observed truncation was subtle in morphants and did not appear to be the consequence of a malformed Meckel's cartilage or defects in the development of the ceratohyal. However, upon higher magnification, *hspg2* morphants demonstrated an abnormal mandibular jaw joint between the Meckel's cartilage and palatoquadrate (the dorsal component of the mandibular arch), a phenotype that was not present in the random control group (Figure 1A'-B').

nkx3.2 expression is decreased in hspg2 morphants

NK3 homeobox 2 (*nkx3.2)* was first identified in the *Drosophila melanogaster* model (where it is known as *bapx1*) and is part of the NK family of homeobox genes (29). Homologues of the gene have been found in vertebrates and are expressed predominately in the first pharyngeal arch (a developmental structure that gives rise to the mandible), where the gene is essential for proper joint formation (29,30). Knockdown of *nkx3.2* causes abnormal jaw joint phenotypes (primarily fusion phenotypes) in amphibians and zebrafish (29,31). Therefore, we utilized *nkx3.2* expression as a marker of mandibular jaw joint development. *In situ* hybridization performed at 2 DPF (Figures 2A-B) demonstrated decreased expression of *nkx3.2*. *nkx3.2* is primarily expressed in the pharyngeal arches, where we observed high expression in the 1st and 5th pharyngeal arches (Figure 2A'-B') (expressed posterior to the eye, annotated by the black arrow) and in the sclerotomal derivatives (31). Knockdown of *hspg2* resulted in decreased expression of *nkx3.2* in the pharyngeal arches when compared with the random control group. Subsequent qPCR at 4 DPF confirmed a statistically significant decrease in *nkx3.2* in morphants relative to the random control group (Figure 2C).

Neural crest cells migrate normally in the absence of hspg2

Because defects in the number of and migration of NCCs are possible mechanisms by which craniofacial deficits may arise (28), we hypothesized that the craniofacial abnormalities present at 5 DPF might be due to early CNCC defects. To determine if *hspg2* affects early CNCCs, we analyzed *Tg(sox10:TagRFP)* embryos at both the 18 somite (aligning with early NCC specification and migration) (32) and Prim-5 (corresponding with NCCs invading the pharyngeal arches) stages. Cells in the NCC lineage express SRY-box transcription factor 10 (*sox10)* at various stages of development where it maintains their survival, specification, and differentiation (33). Previous studies have used *sox10* expression as a valid marker for visualizing NCCs during early developmental stages (28,34). Results revealed no discernable differences in the location or degree of RFP expression in *hspg2* morphants relative to control (Figure 3A-A' and 3B-B').

dlx2a expression in morphants is unaffected

We next analyzed the expression of distal-less homeobox 2a (*dlx2a)* at the Prim-5 stage in random control and *hspg2* morpholino injected embryos to determine if CNCC specification occurs normally upon knockdown of *hspg2*. This homeobox gene is expressed in cranial neural crest cells migrating to the pharyngeal arches (35) and has been established as a marker of proper CNCC specification (28,34,36). *In situ* hybridization (Figure 4A-C) revealed that there was no significant difference in the expression of *dlx2a* in morphants relative to random control injected and non-injected embryos. qPCR measurements performed at Prim-5 in both RC and MO groups validated the normal level of *dlx2a* expression in morphant animals (Figure 4D). Collectively, these data suggest that early CNCC development was normal.

hspg2 knockdown affects cell numbers in jaw joint region

Based on our results, which suggest that the early NCC lineage was not affected, we next hypothesized that *hspg2* was mediating late stage CNCC differentiation and through this, potentially mediating the

defects found at 5 DPF. To test this, we performed analysis of Sox10^{+} cells at 3 and 4 DPF using *Tg(sox10:TagRFP)* larvae. Chondrocytes across both random control and *hspg2* morphant groups at 3 and 4 DPF had normal morphology and columnar arrangement. Chondrocytes to the left of the joint were more closely clustered together than those on the right and therefore, only cells from 3 rows to the left of the joint were easily discernable as opposed to 5 rows of identifiable cells on the right of the joint.

At 3 DPF (Figure 5A-B), morphants had a statistically significant increase of Sox10^{+} cells at the region of interest (3 rows of chondrocytes to the left of the joint and 5 rows of chondrocytes to the right of the joint) (Figure 5C-C'). Consistent with these results, qPCR detected an increase in *sox10* expression at 3 DPF (Figure 5D). However, at 4 DPF (Figure 6A-B), the number of Sox10^{+} cells were reduced relative to random control injected embryos (Figure 6C-C') and the level of *sox10* expression was approximately 50% of the control according to qPCR (Figure 6D). Subsequent analysis of Col2a1a (collagen, type II, alpha 1a)$^{+}$ cells using the *Tg (col2a1a:EGFP)* transgenic reporter in the mandibular jaw joint region revealed similar chondrocyte morphology and arrangement as samples in the *sox10* group. Cell counts (Figure 7A-B) demonstrated a similar decline in numbers of EGFP+ cells in morphant animals at 4 DPF (Figure 7C-C'). Collectively, these data show a progressive loss of differentiated NCCs between 3 and 4 DPF.

Discussion

Our analysis revealed a 7% mandibular truncation and an abnormal joint phenotype in animals with knockdown of *hspg2*. Deletion of *Hspg2* in mice has been shown to cause truncated snouts, shorter and thicker mandibular structures, and flat faces (13,37,38), but very little has been reported on joint phenotypes and how they pertain to *hspg2* function. Although it is relatively novel, the idea of *hspg2* mediating the mandibular jaw joint region is not unfounded. Similar to other synovial joints, the mandibular jaw joint contains a synovial capsule, which, in previous cell culture work using synovial cells, has been shown to express and require perlecan for proper development (39,40).

The mechanism by which perlecan mediates joint development is currently unknown. However, as discussed in the introduction, perlecan is a multi-domain protein with GAG side chains that interact with various growth factors like BMP, WNT, and FGF— all of which are essential for neural crest development, chondrogenesis, and joint formation (38,40) . Deficiencies or abnormalities in the level of activation of such pathways may account for the decreased number of Sox10+ or Col2a1a+ cells at 4 DPF. Perlecan has also been found to bind to *Ihh* (Indian hedgehog) through its HS side chains, which in turn mediates the proliferation of chondrocytes (38). It should be noted however, that many of these effects and pathways have predominately been implicated in the joints of the appendicular skeleton and that development of the mandibular jaw joint is slightly different.

We further demonstrate that knockdown of *hspg2* is associated with decreased numbers of Col2a1a^{+} cells at 4 DPF. These data suggest that *hspg2* has a function regulating CNCC differentiation, a finding that is supported by the number of Sox10^{+} cells at an equivalent time point. Our studies are supported by previous analysis in mice (*Hspg2*$^{-/-}$) that demonstrated abnormal arrangement and proliferation of

chondrocytes in the appendicular skeleton (13,37). It must be noted however, that although these data support one another, the cells of the appendicular skeleton derive from a different germ layer (the mesoderm) than the cells of the craniofacial skeleton (the ectoderm). Both cell lineages give rise to cartilaginous structures, but the mechanisms by which each population differentiates are likely to be different, prompting further studies. One possible future direction of our work could be to determine the interplay between perlecan and FGF because perlecan binds to FGF-2, which increases the expression of *sox9 in vitro* (39,41). The protein output of *Sox9* in turn is vital to chondrogenesis because it activates *Col2a1* expression in mice (42). It is possible however, that there are various mechanisms underlying the function of *hspg2* in joint development because the HS side chains of perlecan are known to bind to collagen II (12) suggesting a direct function for perlecan in chondrogenesis. Interestingly, we also observed an initial increase in the number of Sox10+ cells at 3 DPF, which at the onset seems to counter the results observed at 4 DPF. However, this increase of cells could be due to a period of proliferation in chondrocytes before maturation followed by increased cell death between 3 and 4 DPF. Further studies in this area are warranted.

Knockdown of *hspg2* was also associated with reduced expression of *nkx3.2* at 4 DPF. These results, when understood in the context of the decrease of Col2a1a^{+} cells found at 4 DPF, appear to match previous results performed in mesenchymal cell culture where *nkx3.2* upregulates *col2a1* by directly binding to the promoter (43). In this situation, diminished expression of *nkx3.2* appears to be directly proportional to a decrease in Col2a1a+ cells and the differentiation of chondrocytes. It is not clear if *hspg2* directly modulates *nkx3.2* expression or if the decreased expression is simply the result of defects in the mandibular jaw joint, but studies performed in the chick have shown that *Nkx3.2* and *Sox9* cooperate to promote chondrogenic differentiation and serve as mediators of Sonic Hedgehog (Shh)-induced chondrogenesis (44). This could be one of the mechanisms by which perlecan indirectly mediates the expression of *nkx3.2* and it would prove to be a novel discovery. Recently, it was shown that *nkx3.2* null animals are viable, making it possible to study this gene in relation to *hspg2* without early lethality (45).

In this paper, we used morpholino-mediated knockdown of *hspg2* in zebrafish as an alternative animal model to study the role of *hspg2* during craniofacial development. Induced knockouts in the murine model have resulted in embryonic lethality from mass hemorrhaging in the pericardial cavity and severe chondrodysplasia, both occurrences which can be temporarily circumvented in the developing zebrafish (26). To circumvent these limitations, three additional mouse models have been produced: the first model lacks exon 3, causing loss of the 3 HS side chains (7), the second is modeled after an SJS patient mutation where there is a G to an A substitution theorized to cause a misfolded protein (37,46), and the third is a model where early lethality is restored via tissue specific expression of *Hspg2* in chondrocytes (47).

While the first two models are viable and can be used to examine adult skeletal phenotypes, the first is centered around exploring the loss of only one domain and the second is mimicking more subtle phenotypes associated with SJS. Our project seeks to understand the role of perlecan in craniofacial

development using a null phenotype, a feat not easily done in a murine model. Zebrafish allow for this type of exploration because unlike mice, they are externally fertilized. This external fertilization enables the study of craniofacial development at early developmental stages, particularly with the use of transgenic fish to target specific genes (48,49). The third model described restores early lethality using a chondrocyte promoter and consequently cannot be utilized to study chondrogenesis or craniofacial development (47). Zebrafish craniofacial development is conserved and the development of the viscerocranium, including the development of the pharyngeal arches, the migration and specification of NCCs, their differentiation, and signaling pathways involved have all been well characterized (24,50). Additionally, because the zebrafish mandibular joint is a synovial joint which develops in a similar fashion to other vertebrate synovial joints, the uncovered mechanisms of this research could be translational to other models (51).

Zebrafish are remarkably easy to manipulate genetically and have been used to great success in genetic studies. The zebrafish genome shares a high degree of genetic similarity with humans and thus provides a manner in which to understand gene function and mechanisms (25). 70% of human genes have one zebrafish ortholog and 82% of the genes associated with morbidity also have at least one zebrafish ortholog (52). CRISPR mutagenesis has emerged as a manner of genetic manipulation readily tolerated in the zebrafish (53) and future studies developing a germline non-sense mutant of *hspg2* are warranted.

All work reported here has been completed by use of a single translation-blocking morpholino. While translation-blocking morpholinos are a simple and effective way in which to knockdown genes of interest, they have been associated with off target effects and non-specific cell death. We recognize that utilization of a single translation-blocking morpholino is a primary limitation to our approach. The *hspg2* open reading frame is very large and difficult to perform mRNA restoration experiments with; this limited our ability to restore the morphant phenotype. In addition, we designed a splice inhibiting morpholino to the 3’ splice acceptor of exon 2, but the designed morpholino did not delete exon 3 as predicted, even at the highest concentration injected (2nl of a 0.9mM stock solution). We did, however, utilize a random control morpholino to account for the possibility of morpholino-induced cell death, an endeavor that proved to be rather successful in previous studies (54,55). And, while injection of HS side chains is a potential rescue for the morphant phenotype we observe, there is the possibility that HS/heparin co-injection would fail to rescue because a domain outside of domain I is also essential for regulation of CNCCs. Therefore, such an experiment is unlikely to demonstrate a full rescue. Collectively, these limitations reveal a potential caveat to our work in that we study a morpholino-derived phenotype. However, our data with one morpholino is supported by previous studies, including those completed using the murine model (13,37). In these studies, numbers of chondrocytes in the lateral skeleton are depleted, chondrocytes congregate abnormally, and mutant mice exhibit craniofacial abnormalities. Ultimately, the work herein, like many other morphant phenotypes provides a rationale for the creation of a germline mutant of *hspg2*.

Despite the limitations to our work, we demonstrate an additional function of *hspg2* in craniofacial development by examining the mandibular jaw joint region specifically. We understand that a germline

mutant would help to substantiate our work, but our data is supported by previous studies, suggesting that what we observed is not a consequence of off-target effects. Nevertheless, future studies are required.

Conclusion

In summary, our results have created novel implications for the role of *hspg2* in the development of the mandibular jaw joint, a region of the craniofacial skeleton for which development has not been well elucidated. Furthermore, connections between *hspg2* and *nkx3.2* have yet to be drawn in literature. Additional data concerning late CNCC differentiation raises pertinent questions about the fate of certain cells within different areas of the developing face. Although future studies to more cohesively understand the role of *hspg2* in craniofacial development are needed, these data lay significant groundwork for future experiments in this field and suggest that zebrafish are an acceptable model to study the function of *hspg2* in craniofacial development.

Methods

Animal Care

For all experiments, embryos were obtained by crossing adult *Tg(sox10:tagRFP)*, *Tg*(*col2a1a*:*EGFP*), or AB wildtype fish. Embryos were maintained in E3 embryo medium at 28˚C. All zebrafish were maintained at The University of Texas El Paso according to the Institutional Animal Care and Use Committee (IACUC) guidelines protocol 811689-5. All adult fish were obtained from the University of Colorado, Anschutz Medical Campus or the Zebrafish International Resource Center (ZIRC). Adult and larval zebrafish were euthanized and anesthetized according to guidelines from the American Veterinary Medical Association and approved IACUC protocols. For euthanasia, adults beyond the age of peak breeding age (>1.5 years old) were euthanized using a solution of 10g/L buffered solution of pharmaceutical grade MS 222. Fish were emerged in solution for 30 minutes at RT. All euthanized adults underwent secondary euthanasia with a cold ice bath (2-4 degrees C). Cessation of movement was indicative of euthanasia. Embryos (<7 days old) were euthanized using 1-10% sodium hypochlorite solution after being anesthetized in cold ice bath. For any genotyping and before fixation, all fish, adults and larvae, were anesthetized using MS 222 (150mg/L for adults and 300mg/L for embryos). The degree of anesthesia was monitored by operculum movement of adults and cessation of movement for larvae.

Antisense oligonucleotide morpholino design and microinjection

Two antisense oligonucleotide morpholino sequences were designed in conjugation with Gene Tool LLC. The first was a translation blocking morpholino (MO) with the sequence 5’-TATCCTCGCCCCCATTTCTGCCAA-3’, created to bind to the *hspg2* translation start site and sterically knockdown perlecan translation in the developing larvae. The second was a random control morpholino with the sequence 5’-AAAAAAAAAAAAAAAAAAAAAAAA-3’. This random control morpholino was used to

assure that the translation blocking MO microinjections were not causing any form of extraneous cell death as previously described (56).

The initial concentration gradient for the translation blocking morpholino was as follows: 0.10 mM (1.65 ng/embryo), 0.30 mM (4.95 ng/embryo), 0.50 mM (8.25 ng/embryo), and 0.70 mM (11.55 ng/embryo). A high mortality rate not attributed to lack of fertilization was found in larvae injected at higher concentrations (0.50 mM and 0.70 mM) when compared to wildtype group at 1 DPF. Morphant larvae at 0.30 mM exhibited growth delays when examined at 1 DPF (verified through somite counts), prohibiting accurate comparison between morphant and control group. Microinjections were then performed at 1.65 ng per embryo at a volume of 0.52 nL per embryo, a concentration and volume where there was minimal mortality and no growth delay. To ensure the final phenotype was not a consequence of global deformities at later stages, larvae were measured for length using Zeiss software and staged according to length at 3 and 4 DPF.

For all experiments, the morphant experimental group is compared to either a random control group or wildtype non-injected. The randomized control morpholino has been shown through previous literature to have no associated phenotypes, indicating that it does not influence final results and therefore is the appropriate control group for comparison (54,55,57). Thus, for statistical analysis, comparisons were performed using a T-test between the random control group and the morpholino. MOs were injected into embryos at the one cell stage with a stock concentration of 0.10 mM (1.65 ng/embryo) and at a volume of 0.52 nL per embryo as explained above. Wildtype larvae were non-injected and used predominately as a baseline for fertilization rates.

Alcian Blue Staining and Imaging

Zebrafish larvae (aged 5 days post fertilization (DPF)) were fixed in 2% PFA in PBS, pH 7.5 for 1 hour at room temperature (RT). Samples were washed for 10 minutes with 100mM Tris pH 7.5/10mM MgCl2, stained with Alcian blue stain (pH 7.5: 0.4% Alcian blue (Anatech Ltd., MI) in 70% EtOH, Tris pH 7.5 (Fisher, MA), and 1 M MgCl2 (Fisher, MA)), and incubated overnight at RT. Samples were subsequently destained and rehydrated using an EtOH: Tris pH 7.5 gradient as previously described (34). Embryos were bleached (30% H2O2 (Sigma, St. Louis, MO), 20% KOH (Fisher, MA)) for 10 minutes at RT. Samples were washed twice for 10 minutes per wash in wash buffer (25% glycerol/0.1% KOH (Fisher, MA)) and stored at 4ºC in storage buffer (50% glycerol/0.1% KOH (Fisher, MA)) until imaged. The distance between the top of the Meckel's cartilage (the ventral component of the mandibular arch) and the top of the ceratohyal (a pharyngeal arch cartilage) was measured for each embryo as a method to analyze truncation of the Meckel's cartilage, which would be analogous to micrognathia as described previously (28). The final measurement is the distance between the two structures and not the full length of the Meckel's cartilage. Distance measurements were performed using Zeiss software and all distances are in uM. For imaging, a representative sample of the two groups (*hspg2* morphants and random control larvae) were dissected and viscerocranium was mounted on a glass slide with 100% glycerol. A Leica microscope was used to take high-resolution color images of each sample.

Whole mount in situ hybridization

Whole mount *in situ* hybridization was performed as described by Thisse and Thisse (58). Larvae were harvested and dechorionated at the indicated time point and fixed in 4% paraformaldehyde (Electron Microscopy Sciences, PA) overnight at 4ºC. Larvae were then dehydrated using a methanol: PBS gradient and stored in 100% methanol overnight at -20°C. Embryos were rehydrated using a PBS:Methanol gradient, washed in PBS with 0.1% Tween 20 and permeabilized with proteinase K (10ug/ml) for the time indicated by Thisse and Thisse (58). Permeabilized larvae were prehybridized for 2 hours in hybridization buffer (HB) (50% deionized formamide (Fisher), 5X SSC (Fisher), 0.1% Tween 20 (Fisher), 50 µg/m heparin (Sigma), 500 µg/mL of RNase-free tRNA (Sigma), and 1M citric acid (Fisher). Larvae were then incubated overnight in fresh HB with probe (*dlx2a* and *nkx3.2* at 127 ng) at 70°C. Samples were washed according to protocol, blocked in 2% sheep serum (Sigma) and 2 mg/ml bovine albumin serum (Sigma) for 2 hours at room temperature. Samples were then incubated with anti-DIG Fab fragments (1:10,000) (Sigma) overnight at 4°C. Samples were developed with BM purple AP substrate (Sigma) and imaged with a Zeiss Discovery Stereo Microscope fitted with Zen Software. Statistical analysis was performed using a Fisher's exact test.

Quantitative real time polymerase chain reaction (PCR)

RNA was isolated from a pool of embryos at the indicated time point using Trizol (Fisher) according to manufacturer's protocol. Reverse transcription was performed using a Verso cDNA Synthesis Kit (Fisher) and total RNA was normalized across all samples. PCR was performed using an Applied Biosystem's StepOne Plus machine with Applied Biosystem's software. Sybr green (Fisher) based primer pairs for each gene analyzed are as follows: *dlx2a* fwd CCTCACGCAAACACAGGTTA, *dlx2a* rev TGTTCATTCTCTGGCTGTGC, *nkx3.2* fwd GCAGATTTAGCGGACGAGAC, *nkx3.2* rev GCTTCAACCACCAGCGTTAT, *sox10* fwd ACGCTACAGGTCAGAGTCAC, *sox10* rev ATGTTGGCCATCACGTCATG, *rpl13a* fwd TCCCAGCTGCTCTCAAGATT, and *rpl13a* rev TTCTTGGAATAGCGCAGCTT. Analysis was performed using $2^{\Delta\Delta ct}$ indicating relative mRNA expression for each gene. For each biological replicate, RNA was isolated from a pool of injected embryos. Morphant gene expression changes are demonstrated relative to the expression from a pooled group of individuals injected with random control morpholinos. Each qPCR analysis was performed in biological duplicate, which can be defined as two independent occasions with independent parents and an independent injection, except for the expression of *dlx2a*, which was performed using a single pool of n=10 larvae and was performed to validate *in situ* hybridization. For each biological replicate, the qPCR was performed in technical triplicates, however a single gray dot on the graphs in Figure 2, 5, and 6 demonstrate the average of the three technical replicates and each gray dot represents a different biological replicate. Statistical analysis of messenger RNA (mRNA) expression was performed using a Student t-test on biological replicates, by taking the average and standard deviation of each biological replicate.

Confocal Imaging and Transgenic Cell Counts

Transgenic larvae (*Tg(sox10:tagRFP*) and *Tg(col2a1a:EGFP*)) were fixed at the stated time points using 4% paraformaldehyde. Fixed larvae were mounted in 0.6% low-melt agar in a glass bottom dish (Fisher). Imaging was performed on a Zeiss LSM 700 at 20X and 40X Oil magnification. Images were restricted to the larval craniofacial region. For each fish, a minimum of 20 to 30 z-stacks were collected. At 3 DPF, micron depth across the *Tg(sox10:TagRFP)* random control group ranged from 60-100 μm while micron depth ranged from 57-84 μm in morphants. Micron depth across the 4 DPF *Tg*(*sox10:TagRFP)* random control group ranged from 63-100 μm and from 66-93 μm in the morphant group. At 4 DPF *Tg(col2a1a:EGFP)* random control group micron depth ranged from 63-99 μm and from 72-90 μm in the morphant group.

The number of cells per z-stack (20-30 stacks/fish) at both jaw joints were manually counted using the ImageJ cell counter, which marks each individual cell and keeps track of total cell numbers. Region of interest around the jaw joints were selected to be 3 rows of chondrocytes on the left side of the joint and 5 rows on the right. This region was selected because these cells were consistently visible across z-stacks. Statistical significance was obtained by using a Student t-test with random control and morphant data (59).

Abbreviations

HSPG2/Hspg2/hspg2: heparan sulfate proteoglycan 2; dpf: days-post-fertilization, NCC: neural crest cells; *sox10:* SRY-box transcription factor 10; *nkx3.*2: NK3 homeobox 2; SJS: Schwartz-Jampel Syndrome; DDSH: Dyssegmental Dysplasia Handmaker Type; qPCR: quantitative polymerase chain reaction; *col2a1a:* collagen, type II, alpha 1a; MO: *hspg2* morphants; NI: non-injected wildtype; RC: random control group

Declarations

Ethics approval and consent to participate

All experiments were performed according to protocol 811689-5 approved by The University of Texas El Paso Institutional Animal Care and Use Committee (IACUC).

Consent for publication

Not applicable.

Availability of data and materials

Not applicable.

Competing interests

The authors declare that they have no competing interests.

Funding

National Institute of Neurological Disorders and Stroke 1K01NS099153-01A1 to Anita M. Quintana. This study was designed, performed, and analyzed by the authors. The funding sources provided financial support for the experiments described.

Authors' contributions

BSC and AMQ synthesized hypothesis, wrote manuscript and BSC performed all experiments described. NGR produced aspects of the manuscript figures. All authors included have read and approved the manuscript being submitted.

Acknowledgments

We would like to acknowledge the rest of the Quintana lab members, specifically David Paz and Victoria Castro for their help and support in animal care, aquarium maintenance, and in offering pertinent critical feedback for this project throughout its development.

References

1. Nicole S, Davoine CS, Topaloglu H, Cattolico L, Barral D, Beighton P, et al. Perlecan, the major proteoglycan of basement membranes, is altered in patients with Schwartz-Jampel syndrome (chondrodystrophic myotonia). Nat Genet. 2000 Dec;26(4):480–3.
2. Arikawa-Hirasawa E, Le AH, Nishino I, Nonaka I, Ho NC, Francomano CA, et al. Structural and functional mutations of the perlecan gene cause Schwartz-Jampel syndrome, with myotonic myopathy and chondrodysplasia. Am J Hum Genet. 2002 May;70(5):1368–75.
3. Arikawa-Hirasawa E, Wilcox WR, Le AH, Silverman N, Govindraj P, Hassell JR, et al. Dyssegmental dysplasia, Silverman-Handmaker type, is caused by functional null mutations of the perlecan gene. Nat Genet. 2001 Apr;27(4):431–4.
4. Stum M, Davoine C-S, Vicart S, Guillot-Noël L, Topaloglu H, Carod-Artal FJ, et al. Spectrum of HSPG2 (Perlecan) mutations in patients with Schwartz-Jampel syndrome. Hum Mutat. 2006;27(11):1082–91.
5. Martinez JR, Dhawan A, Farach-Carson MC. Modular Proteoglycan Perlecan/HSPG2: Mutations, Phenotypes, and Functions. Genes [Internet]. 2018 Nov 16 [cited 2019 Oct 26];9(11). Available from: https://www.ncbi.nlm.nih.gov/pmc/articles/PMC6266596/
6. Knox S, Merry C, Stringer S, Melrose J, Whitelock J. Not All Perlecans Are Created Equal INTERACTIONS WITH FIBROBLAST GROWTH FACTOR (FGF) 2 AND FGF RECEPTORS. J Biol Chem. 2002 Apr 26;277(17):14657–65.
7. Rossi M, Morita H, Sormunen R, Airenne S, Kreivi M, Wang L, et al. Heparan sulfate chains of perlecan are indispensable in the lens capsule but not in the kidney. EMBO J. 2003 Jan 15;22(2):236–45.

8. Farach-Carson MC, Warren CR, Harrington DA, Carson DD. Border patrol: insights into the unique role of perlecan/heparan sulfate proteoglycan 2 at cell and tissue borders. Matrix Biol J Int Soc Matrix Biol. 2014 Feb;34:64–79.
9. Gubbiotti MA, Neill T, Iozzo RV. A current view of perlecan in physiology and pathology: A mosaic of functions. Matrix Biol J Int Soc Matrix Biol. 2017 Jan;57–58:285–98.
10. Yang W, Gomes RR, Brown AJ, Burdett AR, Alicknavitch M, Farach-Carson MC, et al. Chondrogenic Differentiation on Perlecan Domain I, Collagen II and Bone Morphogenetic Protein 2-Based Matrices. Tissue Eng. 2006 Jul;12(7):2009–24.
11. Meneghetti MCZ, Hughes AJ, Rudd TR, Nader HB, Powell AK, Yates EA, et al. Heparan sulfate and heparin interactions with proteins. J R Soc Interface [Internet]. 2015 Sep 6 [cited 2020 Aug 6];12(110). Available from: https://www.ncbi.nlm.nih.gov/pmc/articles/PMC4614469/
12. Whitelock JM, Iozzo RV. Heparan Sulfate: A Complex Polymer Charged with Biological Activity. Chem Rev. 2005 Jul 1;105(7):2745–64.
13. Arikawa-Hirasawa E, Watanabe H, Takami H, Hassell JR, Yamada Y. Perlecan is essential for cartilage and cephalic development. Nat Genet. 1999 Nov;23(3):354–8.
14. Costell M, Gustafsson E, Aszódi A, Mörgelin M, Bloch W, Hunziker E, et al. Perlecan Maintains the Integrity of Cartilage and Some Basement Membranes. J Cell Biol. 1999 Nov 29;147(5):1109–22.
15. Gustafsson E, Aszódi A, Ortega N, Hunziker EB, Denker H-W, Werb Z, et al. Role of Collagen Type II and Perlecan in Skeletal Development. Ann N Y Acad Sci. 2003 May 1;995(1):140–50.
16. Bhatt S, Diaz R, Trainor PA. Signals and Switches in Mammalian Neural Crest Cell Differentiation. Cold Spring Harb Perspect Biol [Internet]. 2013 Feb [cited 2020 Aug 6];5(2). Available from: https://www.ncbi.nlm.nih.gov/pmc/articles/PMC3552505/
17. Cordero DR, Brugmann S, Chu Y, Bajpai R, Jame M, Helms JA. Cranial neural crest cells on the move: their roles in craniofacial development. Am J Med Genet A. 2011 Feb;155A(2):270–9.
18. Zhang D, Ighaniyan S, Stathopoulos L, Rollo B, Landman K, Hutson J, et al. The neural crest: A versatile organ system. Birth Defects Res Part C Embryo Today Rev. 2014;102(3):275–98.
19. Graf D, Malik Z, Hayano S, Mishina Y. Common mechanisms in development and disease: BMP signaling in craniofacial development. Cytokine Growth Factor Rev. 2016 Feb;27:129–39.
20. Prasad MS, Charney RM, García-Castro MI. Specification and formation of the neural crest: Perspectives on lineage segregation. Genes N Y N 2000. 2019 Jan;57(1):e23276.
21. Sarkar S, Petiot A, Copp A, Ferretti P, Thorogood P. FGF2 promotes skeletogenic differentiation of cranial neural crest cells. Development. 2001 Jun 1;128(11):2143–52.
22. Melrose J, Smith S, Cake M, Read R, Whitelock J. Perlecan displays variable spatial and temporal immunolocalisation patterns in the articular and growth plate cartilages of the ovine stifle joint. Histochem Cell Biol. 2005 Jun 1;123(6):561–71.
23. Stocum DL, Roberts WE. Part I: Development and Physiology of the Temporomandibular Joint. Curr Osteoporos Rep. 2018 Aug 1;16(4):360–8.

24. Mork L, Crump G. Zebrafish Craniofacial Development: A Window into Early Patterning. Curr Top Dev Biol. 2015;115:235–69.
25. Bradford YM, Toro S, Ramachandran S, Ruzicka L, Howe DG, Eagle A, et al. Zebrafish Models of Human Disease: Gaining Insight into Human Disease at ZFIN. ILAR J. 2017 Jul 1;58(1):4–16.
26. Zoeller JJ, McQuillan A, Whitelock J, Ho S-Y, Iozzo RV. A central function for perlecan in skeletal muscle and cardiovascular development. J Cell Biol. 2008 Apr 21;181(2):381–94.
27. Carrara N, Weaver M, Piedade WP, Vöcking O, Famulski JK. Temporal characterization of optic fissure basement membrane composition suggests nidogen may be an initial target of remodeling. Dev Biol. 2019 Aug 1;452(1):43–54.
28. Quintana AM, Hernandez JA, Gonzalez CG. Functional analysis of the zebrafish ortholog of HMGCS1 reveals independent functions for cholesterol and isoprenoids in craniofacial development. PloS One. 2017;12(7):e0180856.
29. Lukas P, Olsson L. Bapx1 is required for jaw joint development in amphibians. Evol Dev. 2018;20(6):192–206.
30. Walker MB, Miller CT, Swartz ME, Eberhart JK, Kimmel CB. phospholipase C, beta 3 is required for Endothelin1 regulation of pharyngeal arch patterning in zebrafish. Dev Biol. 2007 Apr 1;304(1):194–207.
31. Miller CT, Yelon D, Stainier DYR, Kimmel CB. Two endothelin 1 effectors, hand2 and bapx1, pattern ventral pharyngeal cartilage and the jaw joint. Dev Camb Engl. 2003 Apr;130(7):1353–65.
32. Klymkowsky MW, Rossi CC, Artinger KB. Mechanisms driving neural crest induction and migration in the zebrafish and Xenopus laevis. Cell Adhes Migr. 2010;4(4):595–608.
33. Nelms BL, Labosky PA. Sox Genes [Internet]. Transcriptional Control of Neural Crest Development. Morgan & Claypool Life Sciences; 2010 [cited 2020 Aug 12]. Available from: https://www.ncbi.nlm.nih.gov/books/NBK53136/
34. Quintana AM, Geiger EA, Achilly N, Rosenblatt DS, Maclean KN, Stabler SP, et al. Hcfc1b, a zebrafish ortholog of HCFC1, regulates craniofacial development by modulating mmachc expression. Dev Biol. 2014 Dec 1;396(1):94–106.
35. Sperber SM, Saxena V, Hatch G, Ekker M. Zebrafish dlx2a contributes to hindbrain neural crest survival, is necessary for differentiation of sensory ganglia and functions with dlx1a in maturation of the arch cartilage elements. Dev Biol. 2008 Feb 1;314(1):59–70.
36. LaMonica K, Ding H, Artinger KB. prdm1a functions upstream of itga5 in zebrafish craniofacial development. Genes N Y N 2000. 2015 Apr;53(3–4):270–7.
37. Rodgers KD, Sasaki T, Aszodi A, Jacenko O. Reduced perlecan in mice results in chondrodysplasia resembling Schwartz-Jampel syndrome. Hum Mol Genet. 2007 Mar 1;16(5):515–28.
38. Hassell J, Yamada Y, Arikawa-Hirasawa E. Role of perlecan in skeletal development and diseases. Glycoconj J. 2002 May 1;19(4):263–7.

39. Sadatsuki R, Kaneko H, Kinoshita M, Futami I, Nonaka R, Culley KL, et al. Perlecan is required for the chondrogenic differentiation of synovial mesenchymal cells through regulation of Sox9 gene expression. J Orthop Res Off Publ Orthop Res Soc. 2017;35(4):837–46.
40. Dodge GR, Boesler EW, Jimenez SA. Expression of the basement membrane heparan sulfate proteoglycan (perlecan) in human synovium and in cultured human synovial cells. Lab Investig J Tech Methods Pathol. 1995 Nov;73(5):649–57.
41. Murakami S, Kan M, McKeehan WL, de Crombrugghe B. Up-regulation of the chondrogenic Sox9 gene by fibroblast growth factors is mediated by the mitogen-activated protein kinase pathway. Proc Natl Acad Sci U S A. 2000 Feb 1;97(3):1113–8.
42. Bell DM, Leung KK, Wheatley SC, Ng LJ, Zhou S, Ling KW, et al. SOX9 directly regulates the type-II collagen gene. Nat Genet. 1997 Jun;16(2):174–8.
43. Kawato Y, Hirao M, Ebina K, Shi K, Hashimoto J, Honjo Y, et al. Nkx3.2 promotes primary chondrogenic differentiation by upregulating Col2a1 transcription. PloS One. 2012;7(4):e34703.
44. Rainbow RS, Won HK, Zeng L. The role of Nkx3.2 in chondrogenesis. Front Biol. 2014 Oct;9(5):376–81.
45. Miyashita T, Baddam P, Smeeton J, Oel AP, Natarajan N, Gordon B, et al. nkx3.2 mutant zebrafish accommodate the jaw joint loss through a phenocopy of the head shapes of Paleozoic agnathans. 2019.
46. Lowe DA, Lepori-Bui N, Fomin PV, Sloofman LG, Zhou X, Farach-Carson MC, et al. Deficiency in Perlecan/HSPG2 during Bone Development Enhances Osteogenesis and Decreases Quality of Adult Bone in Mice. Calcif Tissue Int. 2014 Jul;95(1):29–38.
47. Yamashita Y, Nakada S, Yoshihara T, Nara T, Furuya N, Miida T, et al. Perlecan, a heparan sulfate proteoglycan, regulates systemic metabolism with dynamic changes in adipose tissue and skeletal muscle. Sci Rep. 2018 May 17;8(1):7766.
48. Allen JP, Neely MN. Trolling for the ideal model host: zebrafish take the bait. Future Microbiol. 2010 Apr;5(4):563–9.
49. Kwan KM, Fujimoto E, Grabher C, Mangum BD, Hardy ME, Campbell DS, et al. The Tol2kit: a multisite gateway-based construction kit for Tol2 transposon transgenesis constructs. Dev Dyn Off Publ Am Assoc Anat. 2007 Nov;236(11):3088–99.
50. Kimmel CB, Miller CT, Moens CB. Specification and morphogenesis of the zebrafish larval head skeleton. Dev Biol. 2001 May 15;233(2):239–57.
51. Askary A, Smeeton J, Paul S, Schindler S, Braasch I, Ellis NA, et al. Ancient origin of lubricated joints in bony vertebrates. eLife [Internet]. [cited 2020 Aug 18];5. Available from: https://www.ncbi.nlm.nih.gov/pmc/articles/PMC4951194/
52. Howe DG, Bradford YM, Conlin T, Eagle AE, Fashena D, Frazer K, et al. ZFIN, the Zebrafish Model Organism Database: increased support for mutants and transgenics. Nucleic Acids Res. 2013 Jan;41(Database issue):D854–60.

53. Liu K, Petree C, Requena T, Varshney P, Varshney GK. Expanding the CRISPR Toolbox in Zebrafish for Studying Development and Disease. Front Cell Dev Biol [Internet]. 2019 [cited 2020 Aug 13];7. Available from: https://www.frontiersin.org/articles/10.3389/fcell.2019.00013/full
54. Castro VL, Reyes JF, Reyes-Nava NG, Paz D, Quintana AM. Hcfc1a regulates neural precursor proliferation and asxl1 expression in the developing brain. BMC Neurosci. 2020 Jun 10;21(1):27.
55. Reyes-Nava NG, Yu H-C, Coughlin CR, Shaikh TH, Quintana AM. Abnormal expression of GABAA receptor subunits and hypomotility upon loss of gabra1 in zebrafish. Biol Open [Internet]. 2020 Apr 15 [cited 2020 Aug 11];9(4). Available from: https://bio.biologists.org/content/9/4/bio051367
56. Heasman J. Morpholino oligos: making sense of antisense? Dev Biol. 2002 Mar 15;243(2):209–14.
57. Nagashima M, Mawatari K, Tanaka M, Higashi T, Saito H, Muramoto K, et al. Purpurin is a key molecule for cell differentiation during the early development of zebrafish retina. Brain Res. 2009 Dec 11;1302:54–63.
58. Thisse C, Thisse B. High-resolution in situ hybridization to whole-mount zebrafish embryos. Nat Protoc. 2008;3(1):59–69.
59. Hernandez JA, Castro VL, Reyes-Nava N, Montes LP, Quintana AM. Mutations in the zebrafish hmgcs1 gene reveal a novel function for isoprenoids during red blood cell development. Blood Adv. 2019 23;3(8):1244–54.

Figures

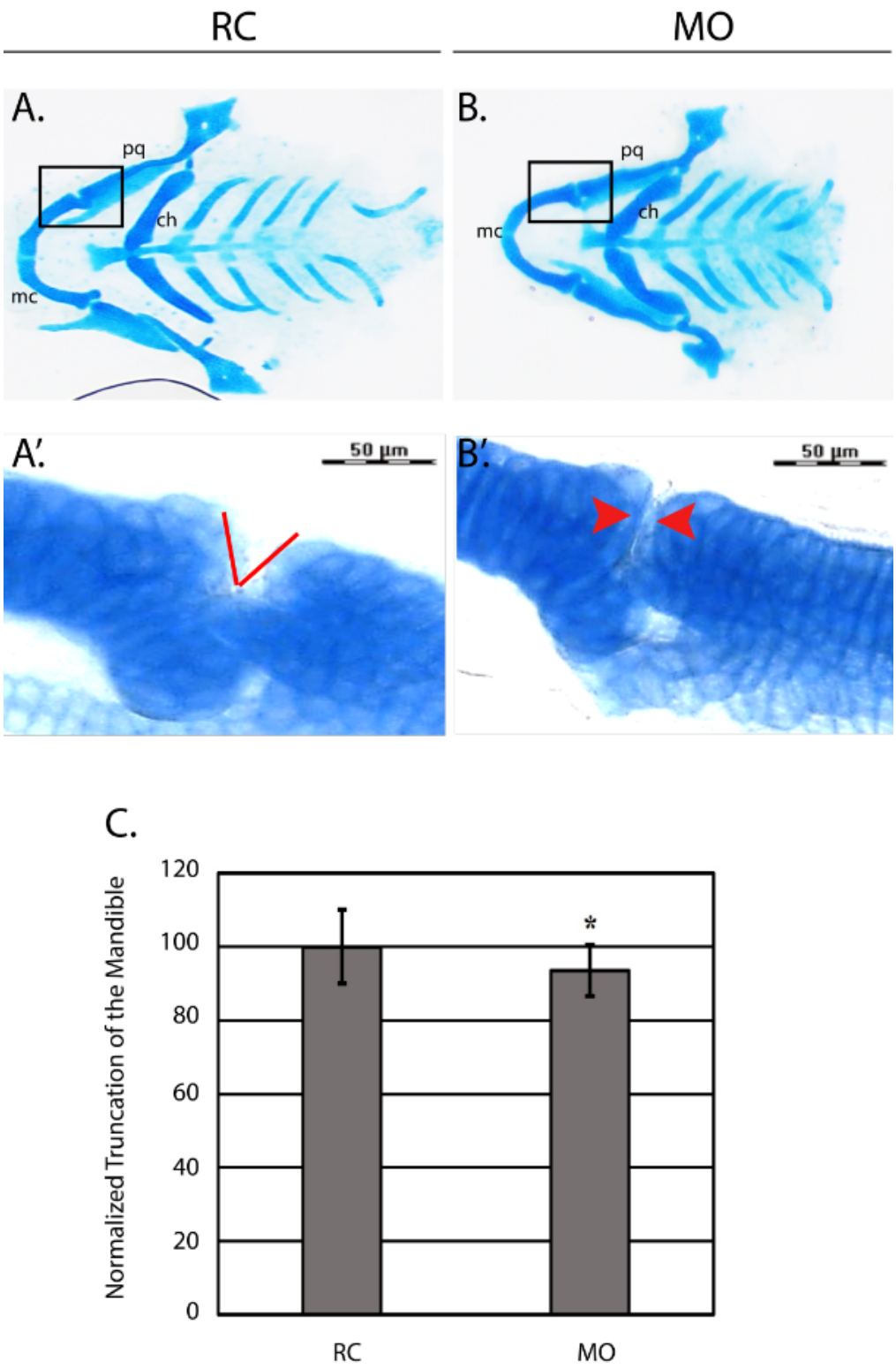

Figure 1

Knockdown of hspg2 is associated with craniofacial phenotypes. (A-B) Random control (RC) and morphant (MO) groups were stained with Alcian blue at 5 days post fertilization (DPF) (N=20 per group). Ceratohyal, Meckel's cartilage, and the palatoquadrate are labeled as the abbreviations (ch), (mc), and (pq) respectively. The black box on each of the images shows the mandibular jaw joint. (A'-B') The mandibular jaw joint enclosed by the black box at 40X magnification. (A') shows a red wedge indicating

the normally developed gap in the mandibular jaw joint and (B') shows two red arrows which indicate an abnormally tight proximity between the two sides of the joint. (C) The distance between the top of the Meckel's cartilage and top of the ceratohyal was measured across both groups (N=20 per group) as a readout for micrognathia. Mandibular length was normalized to the random control (RC) group. *p=0.025.

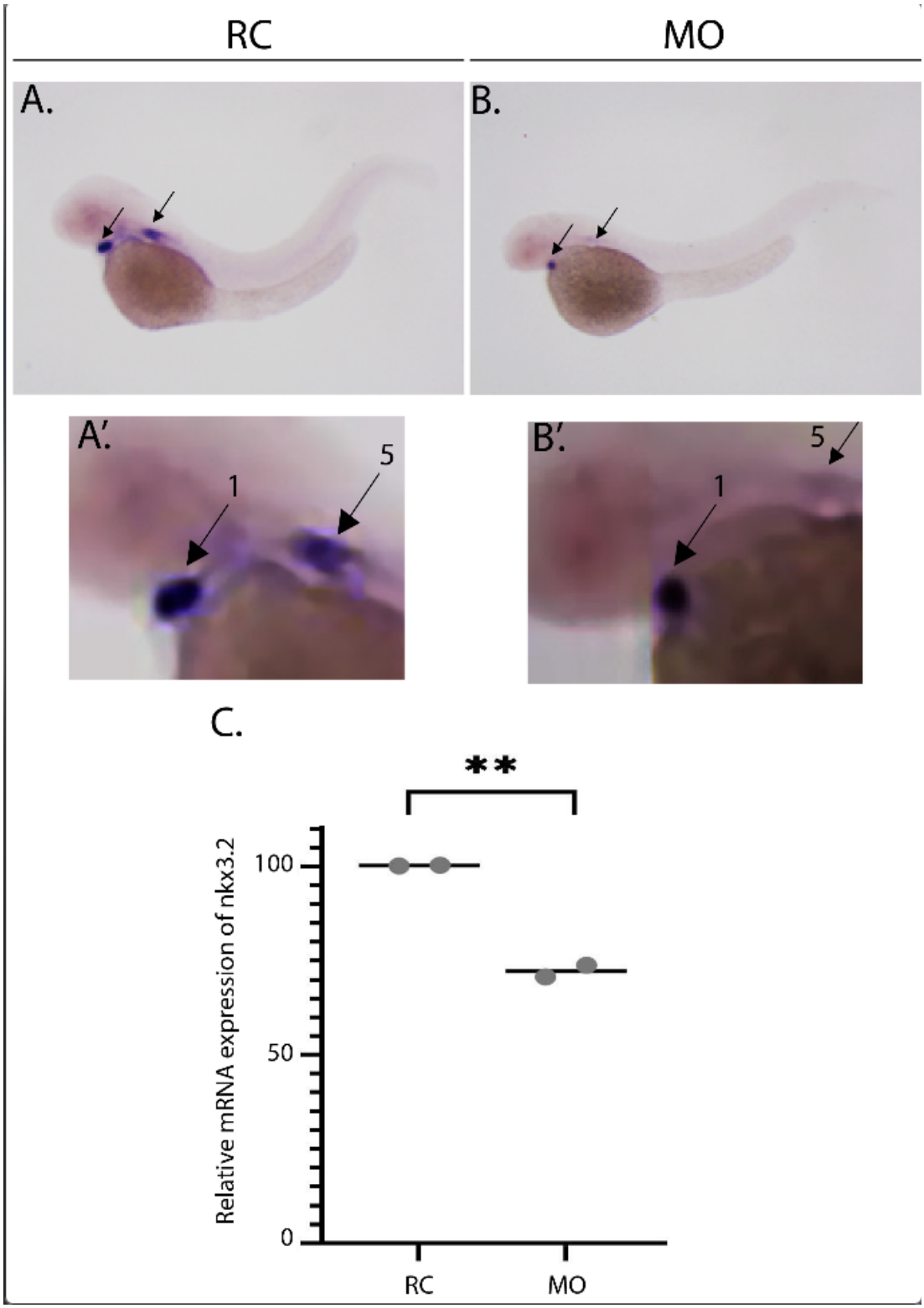

Figure 2

nkx3.2 expression is decreased in hspg2 morphants. (A-B) Whole mount in situ hybridization (ISH) was performed to detect the expression of nkx3.2 at the 2 days post fertilization (DPF) stage. Embryos were injected as described in methods section and subjected to ISH to detect nkx3.2 expression in the developing jaw joint region. Black arrows indicate the expression of nkx3.2. There were N=18 in the random control (RC) group and N=14 larvae in the hspg2 morphants (MO) group. (A'-B') shows regions of nkx3.2 expression. Number one and attached arrow indicate the first pharyngeal arch and number five and attached arrow indicate the fifth pharyngeal arch. (C) qPCR was performed to detect the expression of nkx3.2 at 4 DPF on two independent occasions each represented by a gray dot. Each biological replicate had a minimum of 7 larvae/group and a total n=15 across both replicates. **p=0.004.

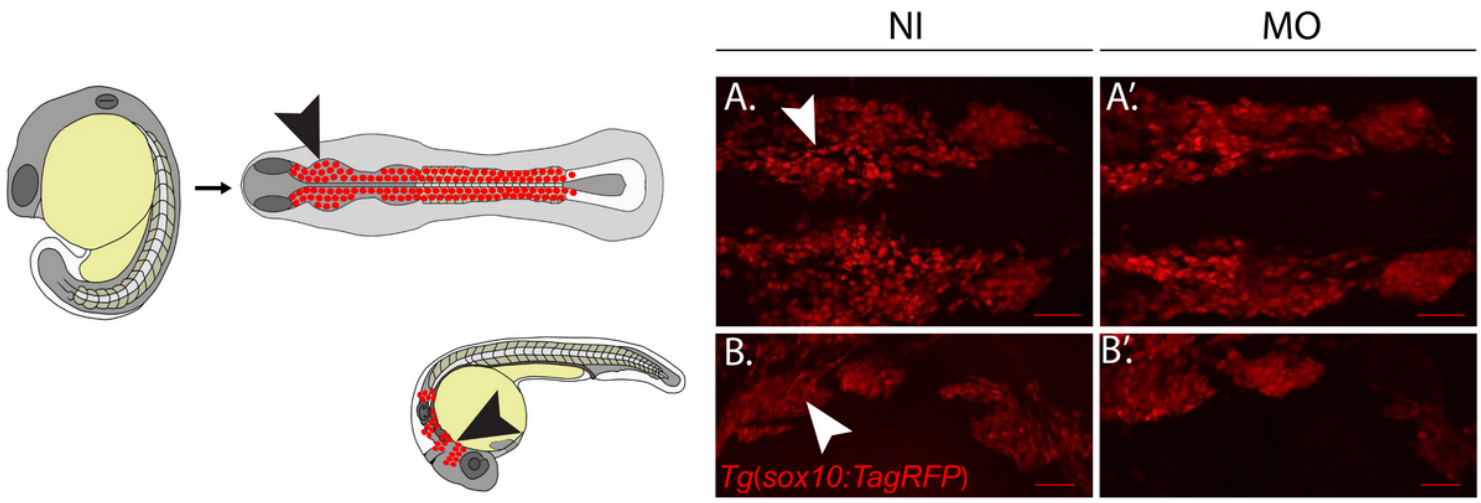

Figure 3

Early neural crest cell (NCC) migration and specification are normal in morphants. (A-A') Non-injected (NI) Tg(sox10:TagRFP) larvae and hspg2 morpholino injected Tg(sox10:TagRFP) larvae (MO) (N=6 and N=4, respectively) larvae were staged and fixed at the 18-somite stage. Images are scaled at 200 μm and demonstrate two lateral streams of Sox10+ migrating NCCs. (B-B') NI and MO larvae (N=8 and N=16 respectively) were staged and fixed at the Prim-5 stage. Images are scaled at 200 μm and demonstrate Sox10+ NCCs in the pharyngeal arches. No significant changes were found between the two groups at either timepoint. Schematic represents the two migratory NCC streams in a zebrafish larva at 18 somites and the localization of the CNCCs in the four pharyngeal arches at the Prim-5 stage.

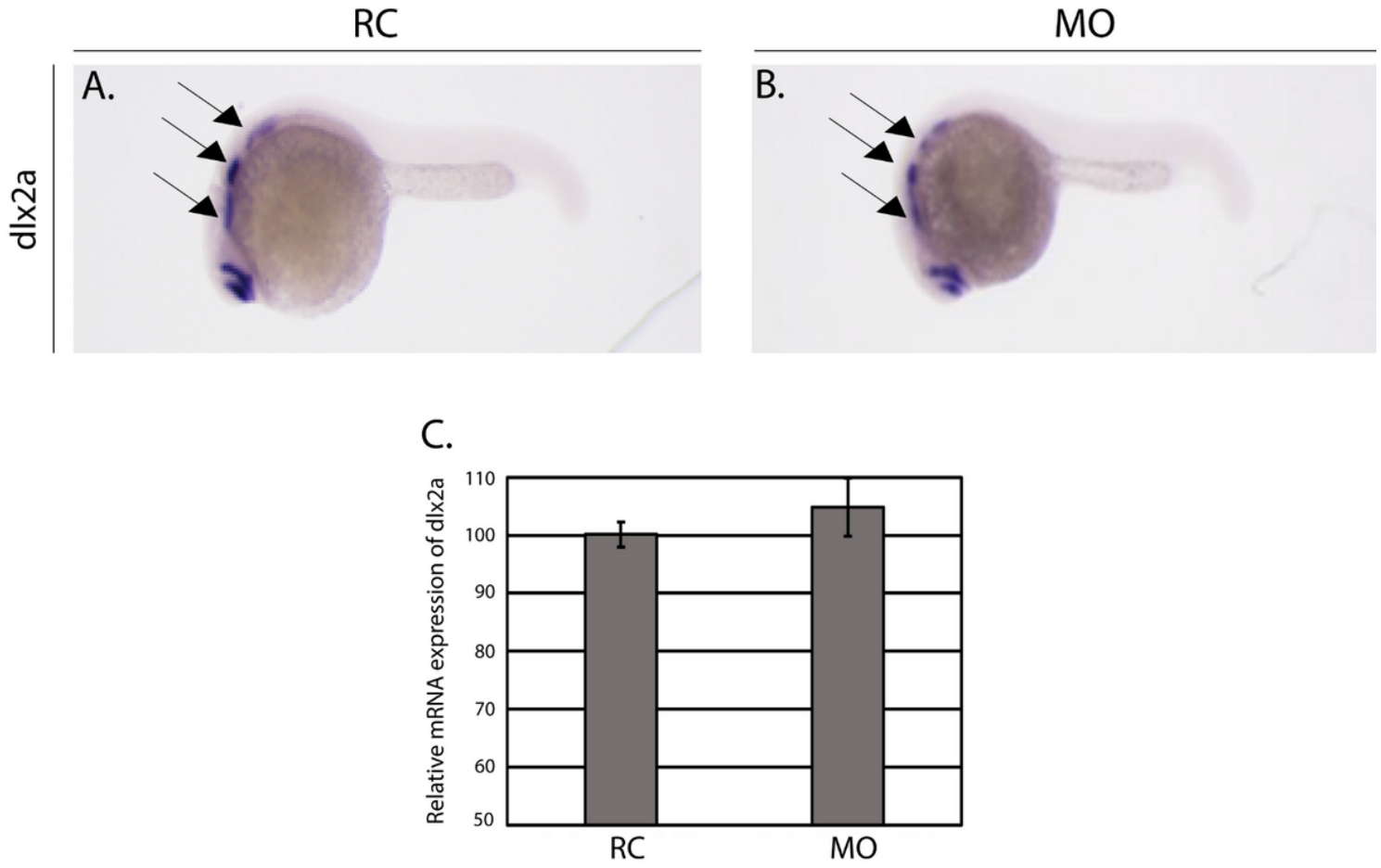

Figure 4

dlx2a expression is normal in morphants. (A-C) Whole mount in situ hybridization (ISH) was performed to detect the expression of dlx2a at the Prim-5 stage (N=10 larvae in non-injected (NI) group, N=12 larvae in random control (RC) group, and N=11 larvae in hspg2 morphant (MO) group). Embryos were injected as described in the methods section and subjected to ISH to detect dlx2a expression in the pharyngeal arches labeled by black arrows. (D) qPCR was performed to detect the expression of dlx2a. Total RNA was isolated from RC and hspg2 MO samples (N=10 per group); error bars represent the standard deviation of technical replicates obtained from a pool of 10 embryos/group.

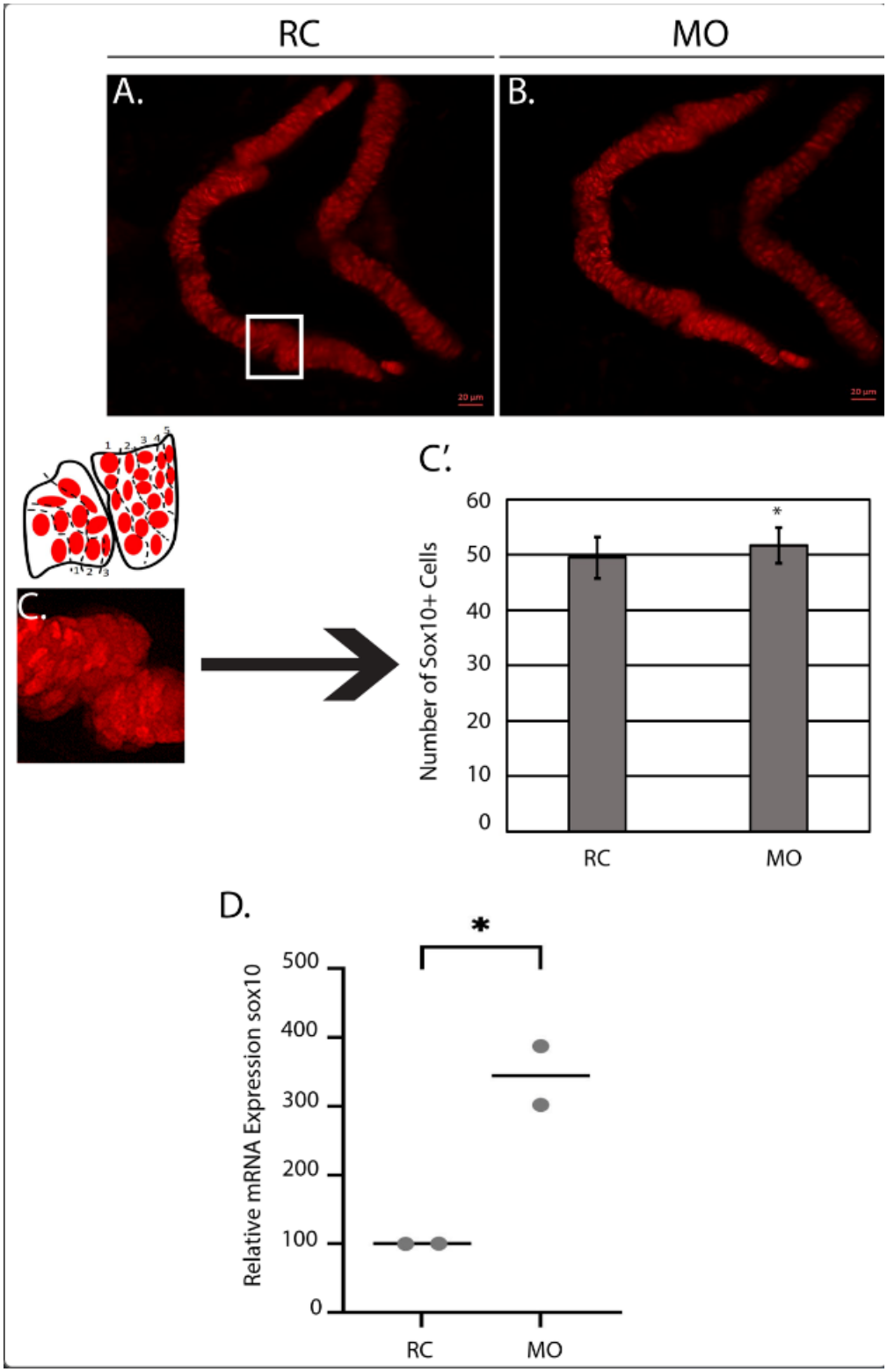

Figure 5

The number of Sox10+ cells is increased in morphants at 3 DPF. (A-B) Tg(sox10:TagRFP) random control (RC) and morphant (MO) larvae (N=10 per group) were mounted in agarose and confocal images were taken at 3 days post fertilization (DPF). (C) shows the representative region where cells were quantified with a corresponding schematic showing the parameters (3 rows left, 5 rows right). (C') Average number of Sox10+ cells counted across both groups (N=10 per group) at 3 DPF. P-value pertains to the

statistically significant difference between the RC group and the MOs (*p= 0.04). (D) qPCR expression of sox10 (N=24 total) in RC and MO groups at 3 DPF (***p=0.0005). qPCR was performed on two independent occasions each represented by a gray dot. Each biological replicate had a minimum of 12 larvae/group for a total n=24.

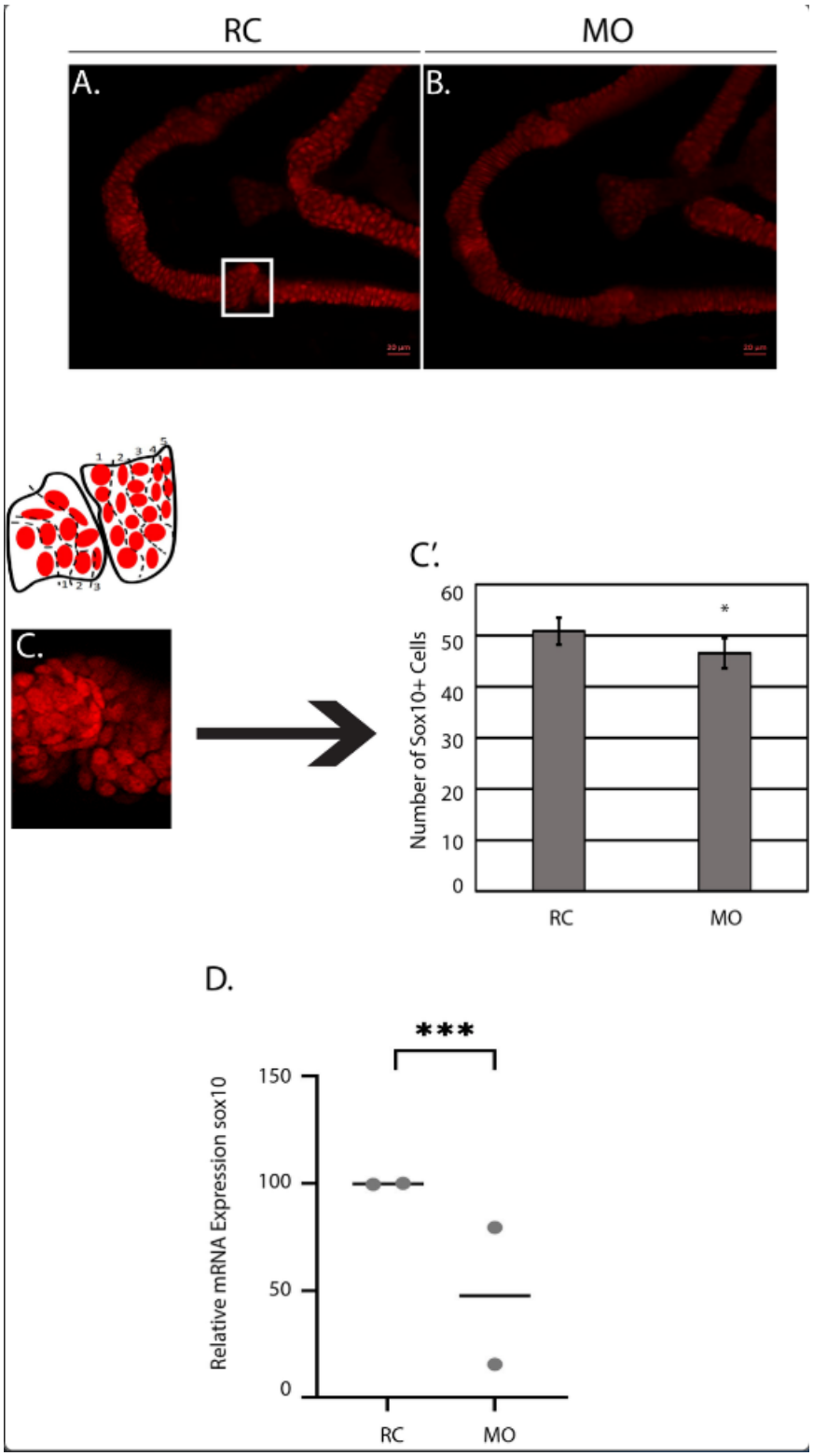

Figure 6

The number of Sox10+ cells is decreased in morphants at 4 DPF. (A-B) Tg(sox10:TagRFP) random control (RC) and morphant (MO) larvae (N=10 per group) were mounted in agarose and confocal images were taken at 4 days post fertilization (DPF). (C) shows the representative region where cells were quantified with a corresponding schematic showing the parameters (3 rows left, 5 rows right). (C') Average number of Sox10+ cells counted across both groups (N=10 per group) at 4 DPF. P-value pertains to the statistically significant difference between the RC group and the MOs (***p=0.0002). (D) qPCR demonstrating the expression of sox10 (N=15 total) in RC and MO groups at 4 DPF (**p=0.005). qPCR was performed on two independent occasions (biological replicates) each represented by a gray dot. Each biological replicate had a minimum of 7 larvae/group and a total n=15.

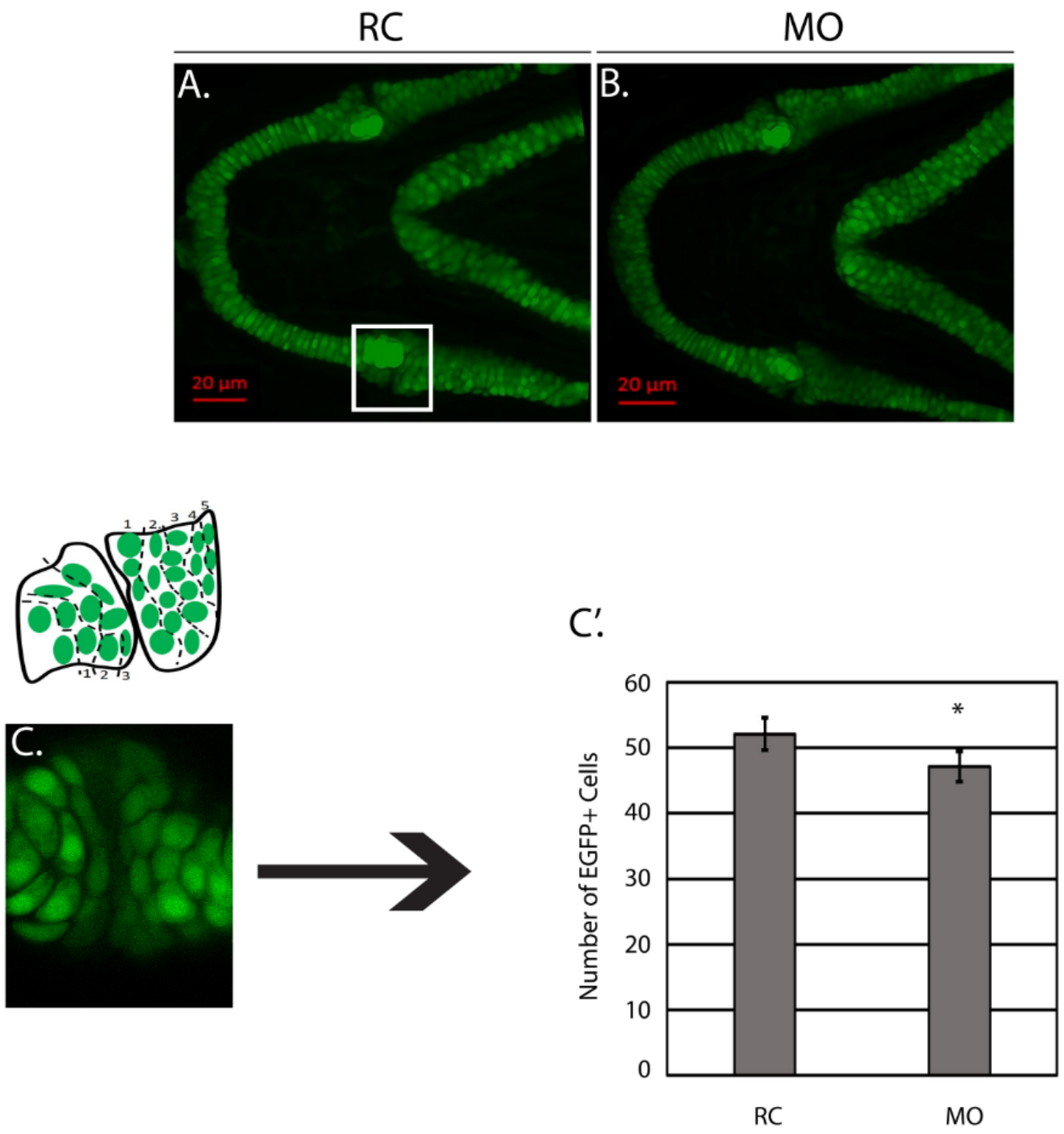

Figure 7

The number of Col2a1a+ cells is decreased at 4 DPF (A-B) Tg(col2a2a:EGFP) random control (RC) and morphant (MO) larvae (N=10 per group) were mounted in agarose and confocal images were taken at 4 days post fertilization (DPF). (C) shows the representative region where cells were quantified with a corresponding schematic showing the parameters (3 rows left, 5 rows right). (C') Average number of

Col2a1a+ cells counted across both groups (N=10 per groups) at 4 DPF. P-value pertains to the statistically significant difference between the RC group and the MOs (***p= 1.44x-05).